JACS
JOURNAL OF THE AMERICAN CHEMICAL SOCIETY
Article
pubs.acs.org/JACS

Characterization of Metastable Intermediates Formed in the Reaction between a Mn(II) Complex and Dioxygen, Including a Crystallographic Structure of a Binuclear Mn(III)−Peroxo Species

Michael K. Coggins,[†] Xianru Sun,[⊥] Yeonju Kwak,[‡] Edward I. Solomon,*[,‡] Elena Rybak-Akimova,*[,⊥] and Julie A. Kovacs*[,†]

[†]Department of Chemistry, University of Washington, Campus Box 351700 Seattle, Washington 98195-1700, United States
[‡]Department of Chemistry, Stanford University, Stanford, California 94305, United States
[⊥]Department of Chemistry, Tufts University, 62 Talbot Avenue, Medford, Massachusetts 02155, United States

Supporting Information

ABSTRACT: Transition-metal peroxos have been implicated as key intermediates in a variety of critical biological processes involving O_2. Because of their highly reactive nature, very few metal−peroxos have been characterized. The dioxygen chemistry of manganese remains largely unexplored despite the proposed involvement of a Mn−peroxo, either as a precursor to, or derived from, O_2, in both photosynthetic H_2O oxidation and DNA biosynthesis. These are arguably two of the most fundamental processes of life. Neither of these biological intermediates has been observed. Herein we describe the dioxygen chemistry of coordinatively unsaturated $[Mn^{II}(S^{Me2}N_4(6\text{-Me-DPEN}))]^+$ (**1**), and the characterization of intermediates formed en route to a binuclear mono-oxo-bridged Mn(III) product $\{[Mn^{III}(S^{Me2}N_4(6\text{-Me-DPEN})]_2(\mu\text{-O})\}^{2+}$ (**2**), the oxo atom of which is derived from $^{18}O_2$. At low-temperatures, a dioxygen intermediate, $[Mn(S^{Me2}N_4(6\text{-Me-DPEN}))(O_2)]^+$ (**4**), is observed (by stopped-flow) to rapidly and irreversibly form in this reaction ($k_1(-10\ °C) = 3780 \pm 180\ M^{-1}\ s^{-1}$, $\Delta H_1^{\ddagger} = 26.4 \pm 1.7$ kJ mol^{-1}, $\Delta S_1^{\ddagger} = -75.6 \pm 6.8$ J mol^{-1} K^{-1}) and then convert more slowly ($k_2(-10\ °C) = 417 \pm 3.2\ M^{-1}\ s^{-1}$, $\Delta H_2^{\ddagger} = 47.1 \pm 1.4$ kJ mol^{-1}, $\Delta S_2^{\ddagger} = -15.0 \pm 5.7$ J mol^{-1} K^{-1}) to a species **3** with isotopically sensitive stretches at $\nu_{O-O}(\Delta^{18}O) = 819(47)\ cm^{-1}$, $k_{O-O} = 3.02$ mdyn/Å, and $\nu_{Mn-O}(\Delta^{18}O) = 611(25)\ cm^{-1}$ consistent with a peroxo. Intermediate **3** releases approximately 0.5 equiv of H_2O_2 per Mn ion upon protonation, and the rate of conversion of **4** to **3** is dependent on [Mn(II)] concentration, consistent with a binuclear $Mn(O_2^{2-})$ Mn peroxo. This was verified by X-ray crystallography, where the peroxo of $\{[Mn^{III}(S^{Me2}N_4(6\text{-Me-DPEN})]_2(\textit{trans-}\mu\text{-}1,2\text{-}O_2)\}^{2+}$ (**3**) is shown to be bridging between two Mn(III) ions in an *end-on trans-μ*-1,2-fashion. This represents the *first characterized example of a binuclear Mn(III)−peroxo*, and a rare case in which more than one intermediate is observed en route to a binuclear μ-oxo-bridged product derived from O_2. Vibrational and metrical parameters for binuclear Mn−peroxo **3** are compared with those of related binuclear Fe− and Cu−peroxo compounds.

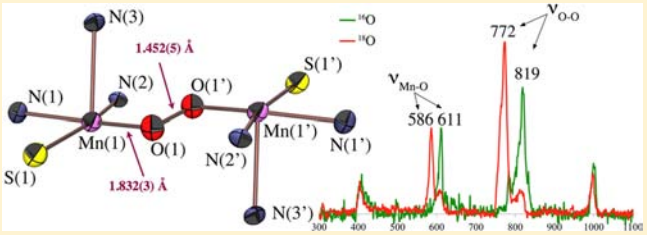

INTRODUCTION

Transition-metal ions promote a wide variety of biochemical processes involving O_2.[1−6] Metal−peroxos are proposed as key intermediates in a majority of these processes.[2,3,7,8] For example, binuclear peroxo-bridged Mn intermediates (Mn−μ-(O_2^{2-})−Mn) are proposed to form during two of the most fundamental processes of life, that of photosynthetic H_2O splitting[9−15] and DNA biosynthesis.[16−18] Photosynthetic H_2O splitting[9−15] generates approximately 80% of the O_2 on our planet. However, neither the photosynthetic Mn−peroxo nor the Mn−peroxo implicated in DNA biosynthesis has been observed. Under extremely high (30 bar) O_2 pressures, a transient Mn species is observed during photosynthetic H_2O splitting;[19] however, the identity of this species is unknown. Although similar peroxo-bridged intermediates are implicated in both of these fundamental processes, one forms from O_2 en route to a more reactive high-valent metal-oxo intermediate,[16−18,20] while the other forms via O−O bond formation from H_2O. Our understanding of the structural and electronic properties that favor O−O bond formation versus cleavage is extremely limited for Mn. Understanding how to efficiently oxidize H_2O to O_2 by examining the microscopic reverse process involving the reduction of dioxygen (O_2) to water (H_2O) should be helpful[21] to the development of renewable solar fuels.[22] Given that it can promote these reactions under mild ambient conditions, Nature has much to teach us. With Cu and Fe, peroxo O−O bond cleavage has been shown to be facilitated either by binding the peroxo between two metal ions, ideally in a *side-on* μ-η^2:η^2-bridging mode,[23−26] or, by protonating one of the oxygens.[27−29] The activation barrier to O_2 binding and activation has been shown to be lowered by

Received: November 13, 2012
Published: March 7, 2013

   dx.doi.org/10.1021/ja311166u | J. Am. Chem. Soc. 2013, 135, 5631−5640

thiolate ligands (RS^-).[30] Thiolate ligands also provide a convenient spectroscopic handle with which to probe reactivity.[31] Despite their key role in biological catalysis, very few Mn−peroxo species have been characterized,[32−43] due, in part, to their instability.[40,44−46] In fact, structurally characterized examples of middle-to-late first-row transition-metal peroxos are, in general, scarce.[1,23,47,48] Of the seven structurally characterized metastable Mn(III)−peroxo compounds,[33,36−39,43] all but one[49] are mononuclear, and five contain the peroxo in a side-on (η^2) binding mode. The only structural evidence for an end-on (η^1) peroxo binding mode with Mn(III) was reported in 1988[49] and more recently by our group.[33] There are only two examples of peroxo-bridged Mn-clusters: one binuclear $Mn(IV)_2$ peroxo compound[40] and one trinuclear $Mn(III)_3$ peroxo compound.[49]

Recently we reported a series of coordinatively unsaturated thiolate-ligated Mn(II) complexes that react with dioxygen, via an observable intermediate, to afford rare examples of unsupported binuclear mono-oxo-bridged Mn(III) complexes.[50] Isotopic labeling studies showed that the oxo atom is derived from O_2.[50] Herein we describe the kinetics of this O_2 reaction and provide evidence that more than one intermediate is involved, one of which is shown to be a binuclear peroxo-bridged Mn(III) complex. Crystallographic characterization of this dioxygen-derived intermediate provides the first structurally characterized example of a binuclear Mn(III)−peroxo. The significance of this structure is that it is analogous to key intermediates proposed to be involved in photosynthetic O_2 evolution and DNA biosynthesis.[9−18,20]

EXPERIMENTAL SECTION

General Methods. All manipulations were performed using Schlenk line techniques or under an N_2 atmosphere in a glovebox. Reagents and solvents were purchased from commercial vendors, were of the highest available purity, and were used without further purification unless otherwise noted. Propionitrile (CaH_2) and MeCN (CaH_2) were dried and distilled prior to use. Et_2O was rigorously degassed and purified using solvent purification columns housed in a custom stainless steel cabinet and dispensed by a stainless-steel Schlenk-line (GlassContour). UV/vis spectra were recorded on a Varian Cary 50 spectrophotometer equipped with a fiber optic cable connected to a "dip" ATR probe (C-technologies). A custom-built two-neck solution sample holder equipped with a threaded glass connector was sized specifically to fit the "dip" probe. Magnetic moments (solid state) were obtained with polycrystalline samples in gel-caps from 5 to 300 K by zero-field cooling experiments using a Quantum Design MPMS S5 SQUID magnetometer. Pascal's constants were used to correct for diamagnetic contributions to the experimental magnetic moment. X-ray crystallography data was recorded on either a Bruker APEX II single crystal X-ray diffractometer with Mo radiation or a Bruker SMART Apex CCD diffractometer with Mo Kα radiation.

Synthesis of Peroxo-Bridged [$Mn^{III}(S^{Me2}N_4$(6-Me-DPEN)]$_2$(trans-μ-1,2-O_2)(BPh_4)$_2$·2CH_3CH_2CN (3). [$Mn^{II}(S^{Me2}N_4$(6-Me-DPEN)](BPh_4) (**1**) was synthesized as previously described for [$Mn^{II}(S^{Me2}N_4$(6-Me-DPEN)](PF_6),[50] by replacing the $NaPF_6$ counterion with $NaBPh_4$. Peroxo-bridged **3** was prepared by cooling a propionitrile solution of **1** to −80 °C, opening the flask to air, and then layering the cold solution with precooled Et_2O.

Hydrogen Peroxide Detection Assay. A concentrated propionitrile solution of **1** (0.1 mL, 5.5 mM) was prepared under an inert atmosphere. After the solution was cooled to −80 °C (with a dry ice/acetone bath), O_2 was gently bubbled into the solution, directly from a cylinder, for approximately 2 min. This procedure promoted a color change from light yellow to dark green, indicating the formation of peroxo-bridged **3**. A minimal amount of concentrated H_2SO_4 (3−4 drops) was then added to the dark green solution, causing the solution to turn clear. The resulting reaction mixture was then passed through a *very* small silica plug, collected, and then added in a single aliquot to a stirring aqueous solution of $KMnO_4$ (3 mL, 6.15×10^{-5} M). The resulting changes in absorbance values were then recorded in 1 min intervals until no further changes were observed. The amount of hydrogen peroxide present was calculated based on the absorbance changes at 550 nm (ε ($M^{-1}cm^{-1}$, 298 K) = 2455) caused by the following reaction:

$$2KMnO_4 + 5H_2O_2 + 6H^+ \rightarrow 2Mn^{2+} + 5O_2 + 8H_2O + 2K^+$$

In a control experiment, the same procedure was performed upon oxo-bridged **2**, which failed to elicit any considerable absorbance changes to aqueous solutions of $KMnO_4$ of known concentration.

Stopped Flow Kinetic Measurements. Acetonitrile solutions of the reagents were prepared in an MBraun glovebox filled with high purity argon and placed in Hamilton gastight syringes. Time-resolved spectra (400−800 nm) were acquired at low temperatures using a TgK Scientific (U.K.) SF-61DX2 Multi-Mixing CryoStopped-Flow Instrument, a J&M TIDASD-AQ diode array detector, and a MCS UV/NIR light source (Spectralytics, Denmark). The stopped-flow instrument was equipped with PEEK tubings fitted inside stainless steel plumbing, a 1.00 cm^3 quartz mixing cell, and an anaerobic kit purged with an inert gas. The temperature in the mixing cell was maintained to 0.1 °C, and the mixing time was 2−3 ms. All flow lines of the instrument were extensively washed with degassed, anhydrous acetonitrile before charging the driving syringes with reactant solutions. The reactions were studied by rapid scanning spectrophotometry under pseudo-first-order conditions with excess oxygen (see experimental details in Supporting Information). Saturated solutions of O_2 were prepared by bubbling dry O_2 gas for 15 min at 25 °C into gastight syringes containing dry CH_3CN; dilutions of the O_2-saturated solvent were performed anaerobically to obtain the desired [O_2]. The solubility of O_2 was taken as 8.1 mM in CH_3CN and at 25 °C.[51] All of the experiments were performed in a single-mixing mode of the instrument, with a 1:1 (v/v) mixing ratio. A series of three or four measurements gave an acceptable standard deviation (within 10%). Data analysis was performed with Kinetic Studio software from Hi-Tech Scientific and IGOR Pro software from Wavemetrics, Inc.

Resonance Raman Experiments. The Raman system consists of a Coherent I90C-K Kr^+ laser, a SPEX model 1877 CP triple monochromator with a filter and blazed holographic gratings of 2400 grooves/mm, and a Newton DU940N-BU 2048 × 512 pixel back-illuminated, thermoelectric-cooled CCD array. Crystalline samples of ^{16}O and ^{18}O-labeled peroxo-bridged **3** were prepared as described above. Spectra were taken at 77 K with 5−40 mW laser power, and the sample was continuously rotated to minimize photodecay.

X-ray Crystallographic Structure Determination. A green needle of **3**, measuring 0.20 × 0.15 × 0.05 mm^3, was mounted on a glass capillary with oil. Data were collected at −173 °C on a Bruker APEX II single crystal X-ray diffractometer, using Mo radiation. The crystal-to-detector distance was set to 40 mm, and the exposure time was 30 s deg^{-1} for all sets of exposure. The scan width was 0.5°. Data collection was 89.4% complete to 25.0° in θ. A total of 27 190 merged reflections were collected covering the indices $h = -15$ to 15, $k = -22$ to 22, $l = -22$ to 22. A total of 7909 reflections were symmetry independent, and R_{int} = 0.0964 indicated that the data were of less than average (0.07) quality. Indexing and unit cell refinement indicated a monoclinic P lattice with the space group as $P2_1/c$ (no. 14).

The data for **3** were integrated and scaled using SAINT and SADABS within the APEX2 software package by Bruker. Solution by direct methods (SHELXS, SIR97) produced a complete heavy atom phasing model consistent with the proposed structure. The structure was completed by difference Fourier synthesis with SHELXL97.[52,53] Scattering factors are from Waasmair and Kirfel.[54] Hydrogen atoms were placed in geometrically idealized positions and constrained to ride on their parent atoms with C···H distances in the range 0.95−1.00 Å. Isotropic thermal parameters (U_{eq}) for the hydrogens were fixed such that they were $1.2U_{eq}$ of their parent atom U_{eq} for methylenes

dx.doi.org/10.1021/ja311166u | J. Am. Chem. Soc. 2013, 135, 5631−5640

and CH's, and 1.5U_{eq} of their parent atom U_{eq} in the case of methyl groups. All non-hydrogen atoms were refined anisotropically by full-matrix least-squares. Crystal data for **3** are summarized in Table 1, and metrical parameters are provided in Tables 2 and 3 below.

Table 1. Crystal Data for $[Mn^{III}(S^{Me2}N_4(6\text{-Me-DPEN})]_2(trans\text{-}\mu\text{-}1,2\text{-}O_2)(BPh_4)_2\cdot 2CH_3CH_2CN$ (3)

formula	$C_{108}\ H_{128}B_2Mn_2N_{14}O_2S_2$
MW	1849.86
T, K	100(2)
unit cell[a]	monoclinic
a, Å	14.2799(10)
b, Å	18.3957(14)
c, Å	18.5282(13)
α, deg	90
β, deg	94.541(2)
γ, deg	90
V, Å^3	4851.9(6)
Z	2
d(calcd), g/cm^3	1.266
space group	$P2_1/c$
R	0.0613[b]
R_w	0.1614[b]
GOF	1.002

[a]In all cases: Mo Kα (λ = 0.71070 Å) radiation. [b]$R = \sum||F_o| - |F_c||/\sum|F_o|$; $R_w = [\sum w(|F_o| - |F_c|)^2/\Sigma wF_o^2]^{1/2}$, where $w^{-1} = [\sigma_{count}^2 + (0.05F^2)^2]/4F^2$.

Two highly disordered propionitriles were found to cocrystallize with peroxo-bridged $[Mn^{III}(S^{Me2}N_4(6\text{-Me-DPEN})]_2(trans\text{-}\mu\text{-}1,2\text{-}O_2)(BPh_4)_2\cdot 2CH_3CH_2CN$ (**3**): one modeled over two positions (83/17 ratio) and the second modeled over three positions (66/17/17 ratio). The occupancies of each disorder component were refined freely while restraining the total occupancy sum to one. Disorder in one of the phenyl rings of the tetraphenylborate anion was modeled over two positions (66/34 ratio) without any additional restraints.

RESULTS AND DISCUSSION

Coordinatively unsaturated $[Mn^{II}(S^{Me2}N_4(6\text{-Me-DPEN}))](BF_4)$ (**1**) was synthesized and structurally characterized as previously described.[50] Dioxygen addition to **1** at ambient temperature causes an immediate color change, from colorless to purple, which is accompanied by the growth of a peak at 560 nm (ε = 520 M^{-1} cm^{-1}) in the electronic absorption spectrum (Figure 1). Crystallization of the product and characterization by X-ray crystallography showed the final purple O_2-derived product to be a rare example of a stable unsupported mono-oxo-bridged binuclear Mn(III) compound, $[Mn^{III}(S^{Me2}N_4(6\text{-Me-DPEN})]_2(\mu\text{-O})(BF_4)_2$ (**2**) (Scheme 1).[50] ^{18}O-labeling studies[50] showed that the bridging oxo atom (blue, Scheme 1) of **2** is derived from dioxygen. When this reaction is monitored at low temperatures (−40 °C, in MeCN) via

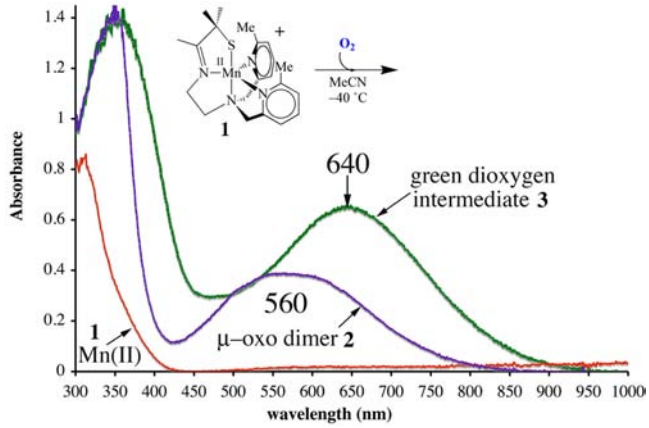

Figure 1. Electronic absorption spectrum of thiolate-ligated $[Mn^{II}(S^{Me2}N_4(6\text{-Me-DPEN}))]^+$ (**1**), the reaction product **2**, and intermediate **3**, formed in its low-temperature reaction with dioxygen (O_2) in MeCN.

electronic absorption spectroscopy, a green metastable intermediate, **3**, is detected, which displays an absorption band at 640 nm (ε = 830 M^{-1} cm^{-1}) (Figure 1). The BF_4^- salt of this intermediate converts to oxo-bridged **2** within minutes at −40 °C. If the BF_4^- or PF_6^- counterion is replaced with BPh_4^-, then the low-temperature (−40 °C) lifetime of **3** can be extended (to ∼45 min) in MeCN. The conversion of **3** to oxo-bridged **2** is nearly quantitative (96−98%) with either counterion, based on the amount of Mn(II) starting material, implying that metastable **3** is well-behaved and cleanly converts to **2**. Low-temperature addition of H_2SO_4 to in situ-generated solutions of **3** reproducibly affords 0.43(4) equiv of H_2O_2 per equiv of Mn^{2+}, as detected and quantified via a MnO_4^- titration using the method described in the experimental section and Figure S-1, Supporting Information. The reproducible observation of hydrogen peroxide in a 2:1 ($Mn:H_2O_2$) stoichiometry suggested that metastable **3** is a bimetallic peroxo, Mn−(μ-O_2^{2-})−Mn.

Although there is only one reported example of a resonance Raman-characterized Mn−peroxo species,[34,49] we were able to successfully perform these experiments using crystalline samples of **3**. Resonance Raman spectra were collected using a series of excitation wavelengths, and resonance enhanced ν_{O-O} and ν_{Mn-O} vibrations are only observed when an excitation frequency of 413 nm near the high energy absorption band of **3** (at 385 nm) is used. Excitation wavelengths near the lower energy visible band (at 640 nm; Figure S-2) did not, on the other hand, result in resonance-enhanced peroxo vibrations, indicating that the higher energy, as opposed to lower energy band, corresponds to a peroxo-to-metal charge transfer band. This is in contrast to iron−peroxo compounds, which display a

Scheme 1

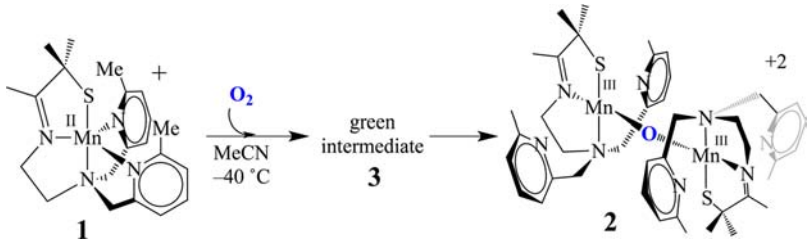

dx.doi.org/10.1021/ja311166u | J. Am. Chem. Soc. 2013, 135, 5631−5640

Table 2. Comparison of Vibrational and Metrical Parameters for Selected Metal−Peroxo Complexes

complex	ν_{O-O}, cm^{-1}	O−O, Å	peroxo binding mode	reference
$[Mn_2(S^{Me2}N_4(6\text{-Me-DPEN}))_2(O_2)]^{2+}$ (**3**)	819	1.452(5)	*trans*-μ-1,2	this work
$[Mn(3,5\text{-iPr}_2\text{pzH})\{(HB(3,5\text{-iPr}_2\text{pz})_3\}(O_2)]$	892	1.428(7)	*side-on* η^2	37
$[Mn(H_3\text{bupa})(O_2)]^-$	885	N/A	*side-on* η^2	35
$[Mn(\text{tmc})(O_2)]^+$	N/A	1.403(4)	*side-on* η^2	43
$[Fe_2(O_2)(O_2CCH_2Ph)\{(HB(pz')_3\}_2]$	888	1.408(9)	*trans*-μ-1,2	7, 76
$[Fe_2(O)_2(\text{N-Et-hptb})(Ph_3PO)_2)_2]^{3+}$	900	1.416(7)	*cis*-μ-1,2	61, 63
$[Fe_2(6\text{-Me}_2\text{-BPP})_2(OH)(O_2)]^+$	908	1.396(5)	*cis*-μ-1,2	59
$[Cu_2(\text{tmpa})_2(O_2)]^+$	825	1.432(6)	*trans*-μ-1,2	26, 63, 64
$[Cu_2(Me_6\text{-tren})_2(O_2)]^{2+}$	814	1.368(9)	*trans*-μ-1,2	92
$[Cu_2\{(HB(3,5\text{-iPr}_2\text{pz})_3\}_2(O_2)]$	741	1.412(12)	μ-η^2:η^2	25, 56
$[Cu_2(\text{MeAN})_2(O_2)]^{2+}$	721	1.540(5)	μ-η^2:η^2	57

peroxo-to-metal charge transfer band in the visible region (at ~700 nm)[20,55] but is in agreement with the TD-DFT-calculated peroxo-to-metal charge transfer transition (π_{op}*(O−O) → Mn(d_{yz})) energies (~450 nm) previously reported for Mn(III)−peroxo complexes $[Mn^{III}(O_2)(L_7py_2^R)]^{2+}$.[34] As shown in Figure 2, isotopically sensitive resonance-enhanced

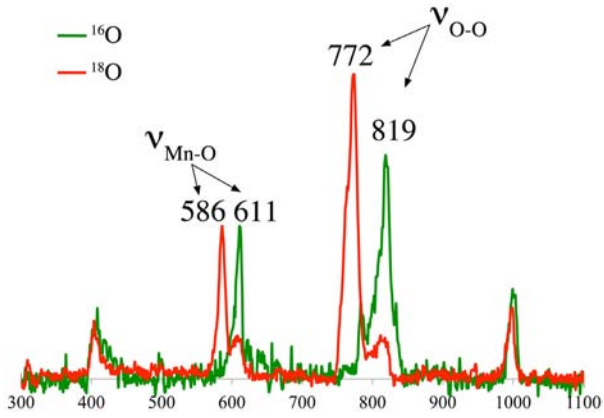

Figure 2. Resonance Raman spectrum of the metastable intermediate **3**, formed in the low-temperature reaction between coordinatively unsaturated $[Mn^{II}(S^{Me2}N_4(6\text{-Me-DPEN}))](BPh_4)$ (**1**) and ^{16}O- (green) and ^{18}O-labled (red) dioxygen (O_2). Counterion (BPh_4^-) stretch seen at 996 cm^{-1}.

vibrations for **3**, not seen with **1** and **2**, are observed at $\nu_{O-O}(\Delta^{18}O)$ = 819(47) cm^{-1} and $\nu_{Mn-O}(\Delta^{18}O)$ = 611(25) cm^{-1}, consistent with a metal−peroxo species. This indicates that two-electron reduction of O_2 has occurred, and the dioxygen O−O bond has been activated. The ν_{O-O} stretching frequency of **3** is significantly lower than the few reported ν_{O-O} frequencies (IR) for monomeric *side-on* Mn(III)−peroxo compounds such as $[Mn(3,5\text{-iPr}_2\text{pzH})\{(HB(3,5\text{-iPr}_2\text{pz})_3\}(O_2)]$ and $[Mn(H_3\text{bupa})(O_2)]^-$ (Table 2).[35,37] A comparison of force constants (vide infra) and an analysis of the coupling between O−O and Mn−O stretches would be necessary in order to comment on the relative extent of O−O bond activation in **3** versus $[Mn(3,5\text{-iPr}_2\text{pzH})\{(HB(3,5\text{-iPr}_2\text{pz})_3\}(O_2)]$ and $[Mn(H_3\text{bupa})(O_2)]^-$; however, this data is not available for the *side-on* Mn(III)−peroxo compounds. Given the known mechanisms for O−O bond activation,[27−29] the low νO−O stretching frequency would suggest that the peroxo of **3** is either protonated or coordinated in a bridging mode. The reproducibly observed 2:1 ratio of H_2O_2:Mn would be more consistent with the latter, and the one example of a vibrationally characterized multinuclear Mn−peroxo compound, $[Mn^{III}_3(\text{dien})_3(\mu\text{-OAc})_2(\mu_3\text{-O})(\text{cis-}\mu\text{-1,2-}O_2)]^{3+}$, also displays a low ν_{O-O} frequency (814 cm^{-1}) consistent with this. Although they are very different in terms of electronic structure, *side-on* binuclear μ-η^2:η^2 Cu peroxo compounds display ν_{O-O} frequencies noticeably lower than that of **3** (Table 2),[25,56,57] whereas *end-on* binuclear Cu−peroxo complexes display ν_{O-O} frequencies comparable to that of **3** (Table 2). Binuclear *end-on* Fe(III)−peroxo species,[55,58−60] including intermediates formed in RNR and MMO,[20] however, show significantly higher ν_{O-O} stretching frequencies (843−908 cm^{-1}) relative to **3** (Table 2). This has been attributed to the large Fe−O−O angles associated with these binuclear Fe(III)−peroxo compounds which induces Fe−O mixing into the O−O bond.[55] The ν_{O-O} stretching frequency for **3** (819 cm^{-1}) does fall in the range (781−844 cm^{-1}) of mononuclear Fe(III) hydroperoxo compounds,[29] where there is no Fe−O mixing into the O−O vibration due to the lack of mechanical coupling.[29,55] As far as vibrations involving the Mn−peroxo bond are concerned, experimentally determined ν_{Mn-O} data are not available for comparison to that observed with **3**.

Verification of the bimetallic nature of peroxo-bound **3** was obtained by X-ray crystallography. Single crystals of the metastable intermediate were obtained by cooling a propionitrile (CH_3CH_2CN) solution of the tetraphenylborate salt of **1** to −80 °C, introducing O_2, and then layering it with Et_2O. As shown by the *R*-factor (6.1%; Table 1) and estimated standard deviations (Table 3), the structure of **3** is of high quality. As shown in the ORTEP diagram of Figure 3, $[Mn^{III}(S^{Me2}N_4(6\text{-Me-DPEN})]_2(\text{trans-}\mu\text{-1,2-}O_2)(BPh_4)_2\cdot 2CH_3CH_2CN$ (**3**) contains an O_2 ligand bridging two manganese ions in an end-on trans configuration (Figure S-3). Each Mn ion is ligated by a thiolate sulfur (S(1)), an O_2-derived oxygen (O(1)), an imine (N(1)), tertiary amine (N(2)), and two N-heterocyclic amine nitrogens (N(3, 4)). The distance separating the pyridine nitrogens N(4) and N(4′) from the Mn ions (2.492(3) Å) is significantly greater than the sum of their covalent radii (2.105 Å).[61] Most likely this is due to Jahn−Teller-like distortion which allows for the stabilization of an antibonding electron. Steric constraints involving the 6-Me substituent and the *gem*-dimethyls adjacent to the sulfur likely contribute as well.[50] The O−O bond length in **3** (1.452(5) Å, Table 3) is significantly longer than that (1.21 Å) of dioxygen (O═O) and close to that of reduced $O-O^{2-}$ (1.49 Å),[48] consistent with reductive activation of the O−O bond. Dioxygen reduction is accompanied by oxidation of both Mn ions in **3** (from the +2 to the +3 oxidation state), as shown by comparison of the Mn−X (X = N, S) bond lengths with those of the reduced starting material **1** and final oxidized product **2** (Table 3).[50]

dx.doi.org/10.1021/ja311166u | J. Am. Chem. Soc. 2013, 135, 5631−5640

Table 3. Selected Bond Distances (Å) and Bond Angles (deg) for Five-Coordinate $[Mn^{II}(S^{Me2}N_4(6\text{-Me-DPEN})](PF_6)$ (1), Oxo-Bridged $[Mn^{III}(S^{Me2}N_4(6\text{-Me-DPEN})]_2(\mu\text{-O})(BF_4)_2\cdot 2MeOH$ (2), and Peroxo-Bound $[Mn^{III}(S^{Me2}N_4(6\text{-Me-DPEN})]_2(trans\text{-}\mu\text{-}1,2\text{-}O_2)(BPh_4)_2\cdot 2CH_3CH_2CN$ (3)

	1	2	3
Mn(1)−S(1)	2.3710(6)	2.2767(7)	2.2747(12)
Mn(1)−N(1)	2.186(2)	1.999(3)	2.040(3)
Mn(1)−N(2)	2.297(2)	2.151(2)	2.203(3)
Mn(1)−N(3)	2.222(2)	2.581(2)	2.410(3)
Mn(1)−N(4)	2.239(2)	2.501(2)	2.492(3)
Mn(1)−O(1)	N/A	1.7602(4)	1.832(3)
O(1)−O(1′)	N/A	N/A	1.452(5)
Mn(1)···O(1′)	N/A	N/A	2.481
Mn(1)···Mn(1′)	N/A	3.520	4.113
Mn(1)−O(1)−O(1′)	N/A	N/A	97.5(6)
O(1)−Mn(1)−S(1)	N/A	95.37	85.12(9)
O(1)−Mn(1)−N(3)	N/A	92.79	92.4(1)
O(1)−Mn(1)−N(1)	N/A	177.21(9)	165.5(1)
O(1)−Mn(1)−N(2)	N/A	100.44(6)	111.1(1)
S(1)−Mn−N(2)	156.98(5)	164.17(7)	163.3(1)
S(1)−Mn−N(3)	117.36(5)	106.2 (1)	109.0(1)
S(1)−Mn−N(4)	117.38(5)	106.84(6)	105.6(1)
N(1)−Mn−N(4)	120.58(7)	92.68(1)	101.7(1)
Mn(1)−O−Mn(1′)	N/A	180.0	N/A

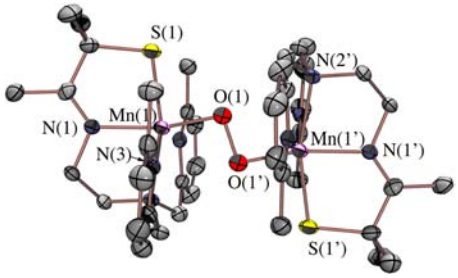

Figure 3. ORTEP of peroxo-bridged $\{[Mn^{III}(S^{Me2}N_4(6\text{-Me-DPEN})]_2(trans\text{-}\mu\text{-}1,2\text{-}O_2)\}^{2+}$ (**3**) showing 50% probability ellipsoids and the atom labeling scheme. Hydrogens have been omitted for clarity.

The Mn(III)−S bond (2.2747(12) Å) of **3** is 0.096 Å shorter than that of reduced **1** but comparable to that of oxidized mono-oxo-bridged $\{[Mn^{III}(S^{Me2}N_4(6\text{-Me-DPEN})]_2(\mu\text{-O})\}^{2+}$ (**2**), $\{[Mn^{III}(S^{Me2}N_4(2\text{-QuinoEN})]_2(\mu\text{-O})\}^{2+}$ (2.292(1) Å), $[Mn^{III}(S^{Me2}N_4(6\text{-Me-DPPN}))]_2(\mu\text{-O})(BPh_4)_2$ (2.255(2) Å), and $\{[Mn^{III}(S^{Me2}N_4(6\text{-H-DPEN})]_2(\mu\text{-O})\}^{2+}$ (2.2968(15) Å),[50] as well as alkylperoxo-ligated $[Mn^{III}(S^{Me2}N_4(2\text{-QuinoEN})(OOtBu)]^+$ (2.270(3) Å).[33] The peroxo in **3** is best described as binding in an *end-on trans*-μ-1,2-O_2 fashion (Figure S-3), as opposed to an asymmetric *side-on* μ-η^2:η^2 fashion as shown by the significantly shorter Mn(1)−O(1) (1.832(3) Å) vs Mn(1)···O(1′) (2.48 Å) distance. *Peroxo-bridged* **3** *represents the first example of a binuclear Mn(III)−peroxo complex*, structurally, or otherwise, characterized. Of the six structurally characterized metastable Mn(III)−peroxo compounds,[33,36,37,39,40] all but one[49] are mononuclear, and five contain the peroxo in a *side-on* (η^2) binding mode. The only other multinuclear Mn(III)−peroxo compound, $[Mn^{III}_3(dien)_3(\mu\text{-OAc})_2(\mu_3\text{-O})(cis\text{-}\mu\text{-}1,2\text{-}O_2)]^{3+}$,[49] contains a bridging *cis*-μ-1,2-peroxo. Aside from this *cis*-μ-1,2-peroxo compound, the only other crystallographically characterized *end-on* manganese−peroxo compound contains an alkyl-peroxo ligand.[33] The Mn−O(1) peroxo bond of **3** is noticebly shorter than all other reported structurally characterized Mn(III)−peroxo compounds (reported range: Mn−O = 1.850(6)−1.901(4) Å).[33,36,37,39,40] The acute Mn−O(1)−O(2) angle (97.5(6)°) indicates that the Mn−O(1) peroxo bond of **3** does not have significant double bond character, however. The peroxo O−O bond of **3** (1.452(5) Å), is significantly longer (Table 2) than all of the structurally characterized *side-on* Mn(III)-η^2-O_2^{2-} (reported range: O−O = 1.410(4)−1.428(7) Å)[36,37,39] but similar in length to the only structurally characterized *end-on* Mn(III)−peroxo compounds, $[Mn^{III}(S^{Me2}N_4(QuinoEN))(OO^tBu)]^+$ (1.457(7) Å),[33] and within the error limits of $[Mn^{III}_3(dien)_3(\mu\text{-OAc})_2(\mu_3\text{-O})(cis\text{-}\mu\text{-}1,2\text{-}O_2)]^{3+}$ (1.6(1) Å).[49] The long peroxo bond length of **3** implies that the O−O bond should be readily cleaved, consistent with its observed conversion to binuclear mono-oxo-bridged **2**. Comparison of the peroxo O−O bond length in binuclear Mn−**3** with selected examples of binuclear Fe− and Cu−peroxo complexes (Table 2) illustrates how the O−O bond length in **3** falls at the high end of that observed in the majority of reactive binuclear metal−peroxo complexes regardless of the peroxo binding mode. This suggests that the peroxo in **3** is highly activated. As shown by a recent analysis of the extremely long (1.540(5) Å) peroxo bond in $[Cu_2(MeAN)_2(O_2)]^{2+}$,[57] a variety of factors (i.e., extent of overlap with the peroxo σ^* vs π^*) influence the peroxo O−O bond length which do not necessarily reflect the extent of O−O bond activation. Another physical parameter which is predictive of the level of O−O bond activation is the vibrational force constant. The force constant associated with the ν_{O-O} of **3** (k = 3.02 mdyn/Å), calculated using normal coordinate analysis, is comparable to those of reactive binuclear Fe− and Cu−peroxo compounds, $[Fe_2(cis\text{-}\mu\text{-}1,2\text{-}O_2)(OBz)_2\{HB(pz')_3\}_2]$ (k = 3.1 mdyn/Å) and $[\{Cu(TMPA)\}_2(trans\text{-}\mu\text{-}1,2\text{-}O_2)]^{2+}$ (k = 3.103 mdyn/Å),[55,62] suggesting that **3** should be reactive as well. The experimentally observed ν_{O-O} stretching frequencies associated with the above Fe− and Cu−peroxo compounds (832 and 876 cm^{-1}),[55,62] on the other hand, are significantly higher than that of **3** (due to the mechanical coupling between the M−O and O−O vibrations) showing that ν_{O-O} stretching frequency cannot be used alone to predict levels of O−O bond activation.[57] The low-temperature (−40 °C) half-life of **3** both in the presence ($\tau_{1/2}$ = 11(2) s; Figure S-4) and in the absence ($\tau_{1/2}$ = 14(2) s) of cyclohexane carboxaldehyde indicates **3** is unreactive toward electrophiles.[35,43] This is in contrast to side-on mononuclear peroxo complexes, $[Mn^{III}(tmc)(O_2)]$,[43] and $[Mn^{III}(H_3bupa)(O_2)]^-$.[35] This lack of reactivity is perhaps not surprising, however, given the bridging, and therefore inaccessible and less nucleophilic, nature of the peroxo in **3**. As shown by the space-filling diagram of Figure 4, the aromatic pyridine rings provide a protective cavity for the peroxo, thus explaining the stability (albeit limited) of what appears to be a highly activated O−O bond. The aromatic rings are roughly coplanar (deviation = 7.95°) with an average C···C separation of 4.16 Å, suggesting that π-stacking interactions might help to stabilize the structure. The crystallographic data show that the Mn^{3+} ions in **3** are significantly more separated (4.113 Å) than would be expected for a bridging *side-on* μ-η^2:η^2-peroxo (~3.5 Å),[23,25,26,47] which is again consistent with an *end-on trans*-μ-1,2-peroxo description. This is a much a less commonly observed peroxo binding

dx.doi.org/10.1021/ja311166u | J. Am. Chem. Soc. 2013, 135, 5631−5640

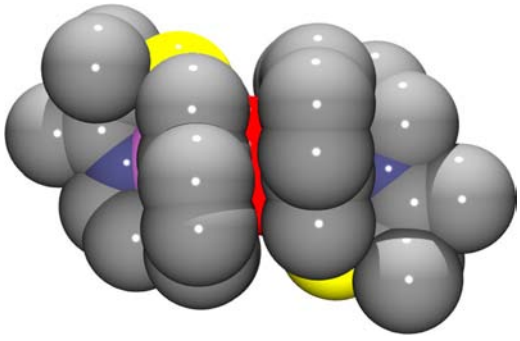

Figure 4. Space-filling diagram of peroxo-bridged $\{[Mn^{III}(S^{Me2}N_4(6\text{-Me-DPEN})]_2(trans\text{-}\mu\text{-}1,2\text{-}O_2)\}^{2+}$, showing that the peroxo (red) is nestled in a protective cavity provided by the pyridine rings.

mode.[63] Fits to the magnetic susceptibility vs temperature (J = 0 cm^{-1}, D = −1.6 cm^{-1}; E/D = 0) curves (Figure 5A), and

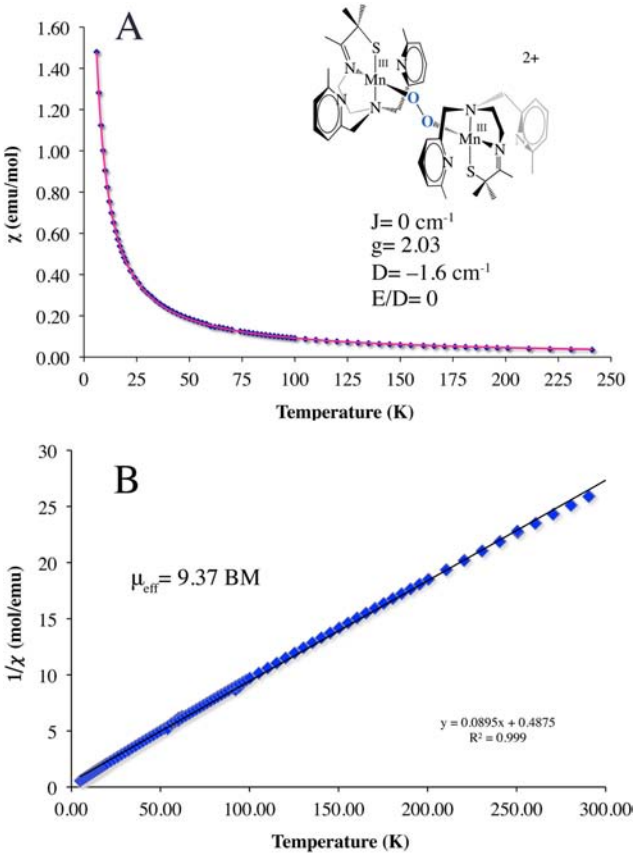

Figure 5. Magnetic susceptibility vs temperature data (A, blue diamonds) obtained for a solid sample of peroxo-bridged $[Mn^{III}(S^{Me2}N_4(6\text{-Me-DPEN})]_2(trans\text{-}\mu\text{-}1,2\text{-}O_2)(BPh_4)_2\cdot 2CH_3CH_2CN$ (**3**). Fits to the chi vs T data (A; pink line; J = 0 cm^{-1}, D = −1.6 cm^{-1}, and E/D = 0),[66] as well as the inverse magnetic susceptibility vs T data (B) are consistent with high spin (S = 2) magnetically uncoupled (down to 5 K) Mn^{3+} ions in an axial environment.

inverse magnetic susceptibility vs temperature data (μ_{eff} = 9.37 μ_B; Figure 5B), indicate that the Mn^{3+} ions of **3** are magnetically uncoupled and high spin (S = 2). Peroxo ligands often mediate strong exchange coupling;[55,64,65] however, DFT single point calculations on the crystal structure of **3** reproduce the low exchange coupling and show that this mainly reflects the fact that the Mn d orbital forming a strong σ-bond with the peroxide π^* orbital is unoccupied. Also, the π-interaction between peroxide and Mn d orbitals is very weak and therefore does not contribute to coupling between the two metal centers.

Kinetics of the Reaction between $[Mn^{II}(S^{Me2}N_4(6\text{-Me-DPEN}))](BPh_4)$ (1) and O_2. To determine the mechanism by which peroxo-bridged $[Mn^{III}(S^{Me2}N_4(6\text{-Me-DPEN})]_2(trans\text{-}\mu\text{-}1,2\text{-}O_2)^{2+}$ (**3**) forms, we examined the kinetics of low-temperature reactions between $[Mn^{II}(S^{Me2}N_4(6\text{-Me-DPEN}))](BPh_4)$ (**1**) and dioxygen. Given the widely accepted proposed mechanisms for binuclear metal−peroxo and μ-oxo formation,[67] the likely mechanism was hypothesized to involve a mononuclear Mn−O_2 intermediate. An intermediate (with λ_{max} = 515 nm) is in fact observed to form on the millisecond time-scale en route to peroxo **3** using a stopped-flow instrument. This intermediate, $[Mn(S^{Me2}N_4(6\text{-Me-DPEN}))(O_2)]^+$ (**4**; Scheme 2), which is presumed to be an η^1-superoxo,

Scheme 2

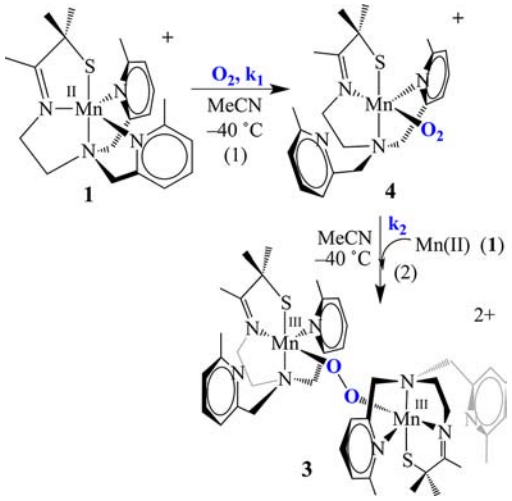

accumulates rapidly (within fractions of a second) in MeCN at low temperatures and then more slowly converts to μ-peroxo-bridged **3** (λ_{max} = 640 nm). Kinetics for both of these steps (shown in Scheme 2) were measured by the stopped-flow technique over the temperature range −40 to −10 °C. A representative spectral overlay is shown in Figure 6, and the general kinetic scheme is shown in eqs 1 and 2:

$$[Mn^{II}] + O_2 \xrightarrow{k_1} [Mn^{III}{-}O_2] \quad (1)$$

$$[Mn^{III}{-}O_2] + [Mn^{II}] \xrightarrow{k_2} [Mn^{III}{-}O_2{-}Mn^{III}] \quad (2)$$

$$\text{rate} = ae^{-k_{1obs}t} + be^{-k_{2obs}t} \quad (3)$$

Kinetic traces (λ = 515 nm) obtained under pseudo-first-order conditions with excess O_2 (Figure 6) were fit to the general two-term rate law shown in eq 3, which represents a general solution to the mechanism outlined in eqs 1 and 2. Pseudo-first-order rate constants, k_{1obs} and k_{2obs}, were obtained (see Supporting Information) by fitting the kinetic traces to eq 3. The observed rate constant associated with formation of intermediate **4**, k_{1obs}, was found to increase linearly with increasing O_2 concentrations, allowing us to determine the second-order rate constant (k_1) from the slope of k_{1obs} vs $[O_2]$ plots. Rate constants were obtained in this manner at four different temperatures (Table 4). The intercepts of the k_{1obs}

dx.doi.org/10.1021/ja311166u | J. Am. Chem. Soc. 2013, 135, 5631−5640

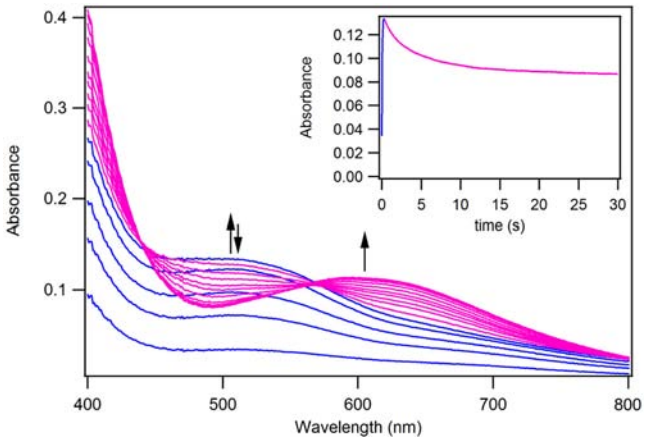

Figure 6. Time-resolved spectral changes obtained upon mixing acetonitrile solutions of Mn(II) complex **1** (1.5 mM) and O_2 (4.05 mM) at −10 °C. Inset: kinetic trace (λ = 515 nm) showing formation and subsequent decay of the Mn−O_2 intermediate **4**. All reported concentrations are after mixing in the stopped-flow cell.

Table 4. Experimentally Measured Temperature-Dependent Rate Constants for the Formation of η^1-Superoxo 4 (k_1) and Binuclear Peroxo-Bridged 3 (k_2) in the Reaction between [$Mn^{II}(S^{Me2}N_4$(6-Me-DPEN))](BPh$_4$) (1) and O_2 in MeCN

temp, °C	k_1, M^{-1} s^{-1}	k_2, M^{-1} s^{-1}
−40	717 ± 45	22.7 ± 0.2
−30	1151 ± 24	60.7 ± 0.3
−20	2106 ± 259	153.6 ± 1.5
−10	3779 ± 180	416.9 ± 3.2

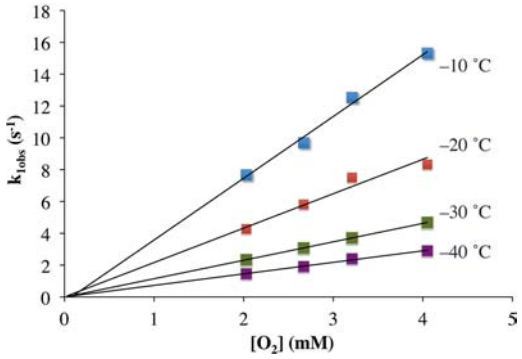

Figure 7. Plots of the observed rate constants (k_{1obs}) for the formation of superoxo intermediate **4** versus O_2 concentration over the temperature range −40 °C to −10 °C in the reaction between Mn(II) complex **1** (1.5 mM) and O_2 in CH_3CN. The slope of each line represents the value of the second-order rate constant for superoxo **4** formation (k_1) at each temperature.

versus O_2 plots were found to be close to zero (Figure 7), indicating that reaction 1 in Scheme 2 is essentially irreversible. The observed rate constant, k_{2obs}, associated with the conversion of superoxo-**4** to peroxo-**3** (rxn (2) in Scheme 2; eq 2), on the other hand, was found to be essentially independent of O_2 concentration over the entire temperature range studied (Figure S-5). This indicates that the rate of formation of the μ-peroxo **3** is zero order in [O_2].

To determine the reaction order with respect to Mn(II) for steps 1 and 2 of Scheme 2 at −30 °C, the [$Mn^{II}(S^{Me2}N_4$(6-Me-DPEN))]$^+$ (**1**) concentration was varied (from 0.8, 1.1, 1.5, to 2.0 mM after mixing) while maintaining a constant amount of excess oxygen (4.1 mM after mixing). The rates of formation of η^1-superoxo **4** and binuclear peroxo-bridged **3** were determined as described above, by following the build-up and decay of **4** at λ = 515 nm. The observed rate constants (k'_{1obs} and k'_{2obs}) were obtained by fitting the kinetic traces to eq 3. The observed pseudo-first-order rate constant for η^1-superoxo intermediate **4** formation (k'_{1obs}) was found to be independent of [Mn(II)] in the presence of excess oxygen, consistent with first-order behavior with respect to [Mn(II)] for step 1 (Figure S-6). Observed rate constants for the formation of μ-peroxo **3** (k'_{2obs}) showed a linear dependence on [Mn(II)] in excess oxygen, confirming second-order behavior with respect to [Mn(II)] overall (Figure 8). This supports the reaction

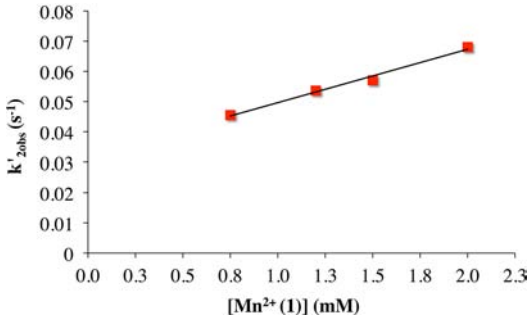

Figure 8. Plot of the observed rate constants (k'_{2obs}) for formation of the binuclear peroxo complex **3** versus [Mn(II)L](BPh$_4$) at −30 °C in CH_3CN. [O_2] after mixing = 4.1 mM.

mechanism outlined in eqs 1 and 2 and Scheme 2. Taken together, the [O_2]- and [Mn(II)]-dependency experiments yield the overall rate law for the formation of superoxo-**4** (eq 4) and peroxo-**3** (eq 5), respectively.

$$\text{rate}_1 = k_1[\text{Mn(II)}][O_2] \quad (4)$$

$$\text{rate}_2 = k_2[\text{Mn(III)}O_2][\text{Mn(II)}] \quad (5)$$

On the basis of the effective second-order dependence on [Mn(II)] for μ-peroxo **3** formation (eq 5), the decay event in kinetic traces at 515 nm was refit to a second-order equation (eq 6) from which k_2 was obtained and used for the calculation of activation parameters.

$$\text{rate}_2 = \text{Abs}_{\text{final}} - [(\text{Abs}_{\text{final}} - \text{Abs}_0)/(1 + k_2[\text{Mn(II)}]_0 t)] \quad (6)$$

The second-order rate constants k_1 and k_2 are summarized over the temperature range −40 °C to −10 °C in Table 4. Activation parameters for the formation of superoxo **4** ($\Delta H_1^{\ddagger}$ = 26.4 ± 1.7 kJ mol^{-1}, $\Delta S_1^{\ddagger}$ = −75.6 ± 6.8 J mol^{-1} K^{-1}) and μ-peroxo **3** ($\Delta H_2^{\ddagger}$ = 47.1 ± 1.4 kJ mol^{-1}, $\Delta S_2^{\ddagger}$ = −15.0 ± 5.7 J mol^{-1} K^{-1}) were obtained from the Eyring plots shown in Figure S-7. The negative entropy of activation would be consistent with an associative process in both steps. The relatively small absolute value of the activation entropy, especially for the second step, may be attributed, at least in part, to desolvation of one (or both) reactants.

Dioxygen binding to iron(II), cobalt(II), and copper(II) is particularly relevant to bioinorganic chemistry, and synthetic model complexes provide important mechanistic insights.[51,68−79] Manganese dioxygen chemistry is, on the other hand, less well developed,[32,35] and no kinetic information is available for comparison to our results. The overall reaction pathway of oxygenation of [$Mn^{II}(S^{Me2}N_4$(6-Me-DPEN))]$^+$ (**1**)

dx.doi.org/10.1021/ja311166u | J. Am. Chem. Soc. 2013, 135, 5631−5640

Table 5. Comparison of Kinetic Parameters for Dioxygen Binding to Mn(II), Fe(II), Cu(I), and Co(II) Complexes

complex	k, M^{-1} s^{-1}	$\Delta H^{\ddagger}$, kJ/mol	$\Delta S^{\ddagger}$, J/K mol	reference
$[Mn^{II}(S^{Me2}N_4(6\text{-Me-DPEN})]^+$ (**1**)	$3.78(18) \times 10^3$ (233 K)[a]	26(2)	−76(7)	this work
$[Fe^{II}_2(HPTP)(O_2CPh)]^{2+}$	$9.6(3) \times 10^2$ (233 K)[c]	16.5(4)[3]	−114(2)	85
$[Fe^{II}_2(OH)_2(TPA)_2]^{2+}$	$1.21(6) \times 10^1$ (233 K)[b]	30(4)[4]	−94(10)	60
$[Fe^{II}_2(OH)_2(6\text{-Me}_3\text{-TPA})_2]^{2+}$	1.94(11) (233 K)[a]	16(2)	−167(10)	60, 86
$[Fe^{II}_2(OH)_2(BQPA)_2]^{2+}$	3.2(2) (233 K)[b]	36(4)	−80(10)	60
$[Fe^{II}_2(OH)_2(BnBQA)_2]^{2}$	$2.67(10) \times 10^3$ (233 K)[a]	16(2)	−108(10)	60
$[Cu^{I}(Me_6\text{-tren})(EtCN)]^+$	$9.5(4) \times 10^4$ (183 K)[c 2]	17.1(6)	−52(3)	93
$[Cu^{I}(TPA)]^+$	$1.50(2) \times 10^8$ (193 K)[d1]	7.62	−45	76, 87, 88
$[Cu^{I}(TPA)(EtCN)]^+$	$5.0(3) \times 10^5$ (223 K)[c]	31.6(5)	10.0(3)	76
$[Cu^{I}(HIPT)_3tren]^+$	2.3(2)[e]	N/A	N/A	90
$[Co^{II}(SalMeDPT)$	8.8×10^4 (203 K)[e]	12.7	−80	89

[a]MeCN. [b]CH_2Cl_2. [c]CH_3CH_2CN. [d]THF. [e]Acetone.

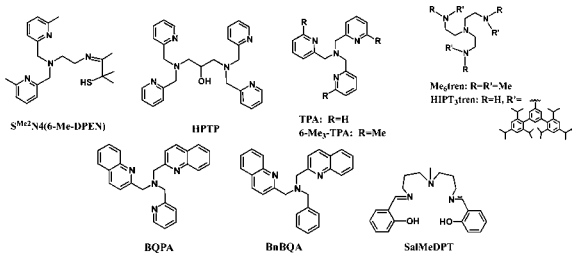

is similar to well-established mechanisms of dioxygen reactivity with other biologically relevant first-row transition-metal complexes.[51,68−74,80−82] Initial coordination of dioxygen to a mononuclear metal complex (Table 5) is often followed by the formation of a dinuclear peroxo species, which in many cases undergoes O−O bond cleavage, to afford either a high-valent mononuclear metal−oxo (M═O) species (Scheme 2) or a high-valent bimetallic bis-μ-oxo ($M(\mu\text{-}O)_2M$) species.[8,26,67,75,83] Steric bulk may, in some cases, stabilize the mononuclear dioxygen adducts and prevent the formation of a dinuclear peroxo complex.[47,71,80,84] The relative rates of individual steps tend to vary as a function of the metal ion and ligand. Kinetic data for O_2 binding to selected examples of aminopyridine or polyamine ligated copper(I), cobalt(II), or iron(II) complexes are listed in Table 5. Although not directly comparable to Mn(II)-containing **1** due to differences in ligand structure and solvent, the activation barrier to O_2 binding to five-coordinate **1** is notably higher than that of coordinatively unsaturated complexes (Table 5). It is comparable, on the other hand, to that of six-coordinate diiron(II) complexes, such as $[Fe_2(HPTP)(O_2CPh)_2]^+$, $[Fe_2(OH)_2(TPA)_2]^{2+}$, or $[Fe_2(OH)_2(BQPA)_2]^{2+}$.[51,86] Oxygen binding to six-coordinate iron(II) further decreases in rate upon increasing the steric bulk of the ligand (e.g., $[Fe_2(OH)_2(6\text{-Me}_3\text{-TPA})_2]^{2+}$).[75,86] Oxygen binding to coordinatively unsaturated Co(II) or Cu(I) is even more rapid (Table 5),[76,87−89] but it can be also retarded by steric hindrance (e.g., $[Cu(HIPT_3)tren]^+$).[90]

CONCLUSIONS

We describe a rare instance in which two metastable intermediates are observed in the low-temperature dioxygen chemistry of a coordinatively unsaturated manganese complex, $[Mn^{II}(S^{Me2}N_4(6\text{-Me-DPEN}))]^+$ (**1**). Although oxygen binding to biologically relevant Fe(II), Cu(I), and Co(II) has been extensively studied,[62,91,92] the observation of more than one intermediate in these processes is relatively rare.[76,87,88,93] Manganese dioxygen chemistry remains largely unexplored.[32,35,40] Low-temperature stopped-flow experiments reported herein show that a dioxygen intermediate, $[Mn^{III}(S^{Me2}N_4(6\text{-Me-DPEN}))(O_2)]^+$ (**4**), rapidly forms upon the addition of O_2 to coordinatively unsaturated **1**, consistent with O_2 binding to an open coordination site. The thiolate ligand helps to maintain an open coordination site.[94] O_2 binding to **1** is found to be relatively slow compared to related biologically relevant Fe and Cu complexes. In the absence of any other kinetic data for O_2 binding to Mn(II), it would be difficult to draw any conclusions regarding the role of the metal ion in this reaction. Dioxygen intermediate **4** was shown to convert more slowly to a species, **3**, with isotopically sensitive stretches in the resonance Raman spectrum ($\nu_{O-O}(\Delta^{18}O)$ = 819(47) cm^{-1}, k_{O-O} = 3.02 mdyn/Å, $\nu_{Mn-O}(\Delta^{18}O)$ = 611(25) cm^{-1}) consistent with a peroxo. The frequency of this ν_{O-O} stretch is compared with that of related binuclear Cu− and Fe−peroxo compounds. Roughly 0.5 equiv of H_2O_2 was shown to be released per Mn ion of **3**, and the rate of conversion of **4** to **3** was shown to be dependent on [Mn(II)] concentration, consistent with its formulation as a binuclear Mn−peroxo. This was verified by X-ray crystallography, where the peroxo of $\{[Mn^{III}(S^{Me2}N_4(6\text{-Me-DPEN})]_2(trans\text{-}\mu\text{-}1,2\text{-}O_2)\}^{2+}$ (**3**) is shown to be bridging between two Mn(III) ions in an *end-on trans-μ*-1,2-fashion. This represents the *first characterized example of a binuclear Mn(III)−peroxo* similar to intermediates proposed to be involved in both H_2O oxidation and DNA biosynthesis, arguably two of the most fundamental processes of life. Neither of these biological intermediates has been observed. The peroxo O−O bond of **3** is shown to be considerably longer than that of all crystallographically characterized mononuclear *side-on* Mn−peroxo compounds and fall at the high end of reported bond lengths for binuclear Cu− and Fe−peroxo compounds, regardless of the peroxo binding mode.

ASSOCIATED CONTENT

Supporting Information

Details regarding the fits to the kinetic traces, quantitative detection of H_2O_2, a quantitative UV/vis of peroxo **3**, ORTEP

dx.doi.org/10.1021/ja311166u | J. Am. Chem. Soc. 2013, 135, 5631−5640

diagram showing connectivity within the dimanganese−peroxo core, half-life dependence on CCA, plots of k_{2obs} vs $[O_2]$, k'_{1obs} vs [Mn(II)], Eyring plots for second-order rate constants k_1 and k_2, and crystallographic tables for peroxo **3**. This material is available free of charge via the Internet at http://pubs.acs.org.

AUTHOR INFORMATION

Corresponding Author

kovacs@chem.washington.edu

Notes

The authors declare no competing financial interest.

ACKNOWLEDGMENTS

J.A.K. gratefully acknowledges the NIH (no. RO1GM45881), E.I.S. gratefully acknowledges NSF Biochemistry (MCB0919027), and E.V.R-A. thanks the US Department of Energy, Office of Basic Energy Science (DE-FG02-06ER15799) for funding.

REFERENCES

(1) Tinberg, C. E.; Lippard, S. J. *Acc. Chem. Res.* **2011**, *44*, 280−288.
(2) Kovaleva, E. G.; Lipscomb, J. D. *Science* **2007**, *316*, 453−456.
(3) Boisvert, L.; Goldberg, K. I. *Acc. Chem. Res.* **2012**, *45*, 899−910.
(4) Zhang, C.; Xu, Z.; Shen, T.; Wu, G.; Zhang, L.; Jiao, N. *Org. Lett.* **2012**, *14*, 2362−2365.
(5) Timokhin, V. I.; Anastasi, N. R.; Stahl, S. S. *J. Am. Chem. Soc.* **2003**, *125*, 12996−12997.
(6) Gottumukkala, A. L.; Teichert, J. F.; Heijnen, D.; Eisink, N.; van Dijk, S.; Ferrer, C.; van den Hoogenband, A.; Minnaard, A. J. *J. Org. Chem.* **2011**, *76*, 3498−3501.
(7) Kim, K.; Lippard, S. L. *J. Am. Chem. Soc.* **1996**, *118*, 4914−4915.
(8) Decker, A.; Solomon, E. I. *Curr. Opin. Chem. Biol.* **2005**, *9*, 152−163.
(9) Umena, Y.; Kawakami, K.; Shen, J.-R.; Kamiya, N. *Nature* **2011**, *473*, 55−60.
(10) Yano, J.; Kern, J.; Sauer, K.; Latimer, M.; Pushkar, Y.; Biesiadka, J.; Loll, B.; Saenger, W.; Messigner, J.; Zouni, A.; Yachandra, V. K. *Science* **2006**, *314*, 821−825.
(11) McEvoy, J. P.; Brudvig, G. W. *Chem. Rev.* **2006**, *106*, 4455−4483.
(12) Kanady, J. S.; Tsui, E. Y.; Day, M. W.; Agapie, T. *Science* **2011**, *333*, 733−736.
(13) Yachandra, V. K.; Sauer, K.; Klein, M. P. *Chem. Rev.* **1996**, *96*, 2927−2950.
(14) Lewis, N. S.; Nocera, D. G. *Proc. Natl. Acad. Sci. U.S.A.* **2006**, *103*, 15729−15735.
(15) Armstrong, F. A. *Philos. Trans. R. Soc. B* **2008**, *363*, 1263−1270.
(16) Zhang, Y.; Stubbe, J. *Biochemistry* **2011**, *50*, 5615−5623.
(17) Boal, A. K.; Cotruvo, J. A., Jr.; Stubbe, J.; Rosenzweig, A. C. *Science* **2010**, *329*, 1526−1530.
(18) Cotruvo, J. A., Jr.; Stubbe, J. *Biochemistry* **2010**, *49*, 1297−1309.
(19) Clausen, J.; Junge, W. *Nature* **2004**, *430*, 480−483.
(20) Skulan, A. J.; Brunold, T. C.; Baldwin, J.; Saleh, L.; Bollinger, J. M., Jr.; Solomon, E. I. *J. Am. Chem. Soc.* **2004**, *126*, 8842−8855.
(21) Eisenberg, R.; Gray, H. B. *Inorg. Chem.* **2008**, *47*, 1697−1699.
(22) Magnuson, A.; Anderlund, M.; Johansson, O.; Lindblad, P.; Lomoth, R.; Plivka, T.; Ott, S.; Stensjo, K.; Styring, S.; Sundstron, V.; Hammarstrom, L. *Acc. Chem. Res.* **2009**, *42*, 1899−1909.
(23) Tolman, W. B. *Acc. Chem. Res.* **1997**, *30*, 227−237.
(24) Solomon, E. I.; Tuczek, F.; Root, D. E.; Brown, C. A. *Chem. Rev.* **1994**, *94*, 827−856.
(25) Kitajima, N.; Fujisawa, K.; Fujimoto, C.; Moro-oka, Y.; Hashimoto, S.; Kitagawa, T.; Toriumi, K.; Tatsumi, K.; Nakamura, A. *J. Am. Chem. Soc.* **1992**, *114*, 1277−1291.
(26) Mirica, L. M.; Ottenwaelder, X.; Stack, T. D. P. *Chem. Rev.* **2004**, *104*, 1013−1045.
(27) Kovacs, J. A. *Science* **2003**, *299*, 1024−1025.
(28) Neese, F.; Solomon, E. I. *J. Am. Chem. Soc.* **1998**, *120*, 12829−12848.
(29) Roelfes, G.; Vrajmasu, V.; Chen, K.; Ho, R. Y. N.; Rohde, J.-U.; Zondervan, C.; Crois, R. M.; Schudde, E. P.; Lutz, M.; Spek, A. L.; Hage, R.; Feringa, B. L.; Munck, E.; Que, L., Jr. *Inorg. Chem.* **2003**, *42*, 2639−2653.
(30) Brown, C. D.; Neidig, M. L.; Neibergall, M. B.; Lipscomb, J. D.; Solomon, E. I. *J. Am. Chem. Soc.* **2007**, *129*, 7427−7438.
(31) Kovacs, J. A.; Brines, L. M. *Acc. Chem. Res.* **2007**, *40*, 501−509.
(32) Shook, R. L.; Peterson, S. M.; Greaves, J.; Moore, C.; Rheingold, A. L.; Borovik, A. S. *J. Am. Chem. Soc.* **2011**, *133*, 5810−5817.
(33) Coggins, M. K.; Kovacs, J. A. *J. Am. Chem. Soc.* **2011**, *133*, 12470−12473.
(34) Geiger, R. A.; Chattopadhyay, S.; Day, V. W.; Jackson, T. A. *J. Am. Chem. Soc.* **2010**, *132*, 2821−2831.
(35) Shook, R. L.; Gunderson, W. A.; Greaves, J.; Ziller, J. W.; Hendrich, M. P.; Borovik, A. S. *J. Am. Chem. Soc.* **2008**, *130*, 8888−8889.
(36) VanAtta, R. B.; Strouse, C. E.; Hanson, L. K.; Valentine, J. S. *J. Am. Chem. Soc.* **1987**, *109*, 1425−1434.
(37) Kitajima, N.; Komatsuzaki, H.; Hikichi, S.; Osawa, M.; Moro-oka, Y. *J. Am. Chem. Soc.* **1994**, *116*, 11596−11597.
(38) Singh, U. P.; Sharma, A. K.; Hikichi, S.; Komatsuzaki, H.; Moro-oka, Y.; Akita, M. *Inorg. Chim. Acta* **2006**, *359*, 4407−4411.
(39) Annaraj, J.; Cho, J.; Lee, Y.-M.; Kim, S. Y.; Latifi, R.; de Visser, S. P.; Nam, W. *Angew. Chem., Int. Ed.* **2009**, *48*, 4150−4153.
(40) Bossek, U.; Weyhermuller, T.; Wieghardt, K.; Nuber, B.; Weiss, J. *J. Am. Chem. Soc.* **1990**, *112*, 6387−6388.
(41) Geiger, R. A.; Leto, D. F.; Chattopadhyay, S.; Dorlet, P.; Anxolabéhère-Mallart, E.; Jackson, T. A. *Inorg. Chem.* **2011**, *50*, 10190−10203.
(42) Geiger, R. A.; Wijeratne, G.; Day, V. W.; Jackson, T. A. *Eur. J. Inorg. Chem.* **2012**, *10*, 1598−1608.
(43) Seo, M. S.; Kim, J. Y.; Annaraj, J.; Kim, Y.; Lee, Y.-M.; Kim, S.-J.; Nam, W. *Angew. Chem., Int. Ed.* **2007**, *46*, 377−380.
(44) Bull, C.; Niederhoffer, E. C.; Yoshida, T.; Fee, J. A. *J. Am. Chem. Soc.* **1991**, *113*, 4069−4076.
(45) Hearn, A. S.; Tu, C. K.; Nick, H. S.; Silverman, D. N. *J. Biol. Chem.* **1999**, *274*, 24457−24460.
(46) Groni, S.; Dorlet, P.; Blain, G.; Bourcier, S.; Guillot, R.; Anxolabéhère-Mallart, E. *Inorg. Chem.* **2008**, *47*, 3166−3172.
(47) Chufan, E. E.; Puiu, S. C.; Karlin, K. D. *Acc. Chem. Res.* **2007**, *40*, 563−572.
(48) Vaska, L. *Acc. Chem. Res.* **1976**, *9*, 175−182.
(49) Bhula, R.; Gainsford, G. J.; Weatherburn, D. C. *J. Am. Chem. Soc.* **1988**, *110*, 7550−7552.
(50) Coggins, M. K.; Toledo, S.; Shaffer, E.; Kaminsky, W.; Shearer, J.; Kovacs, J. A. *Inorg. Chem.* **2012**, *51*, 6633−6644.
(51) Kryatov, S. V.; Rybak-Akimova, E. V.; Schindler, S. *Chem. Rev.* **2005**, *105*, 2175−2226.
(52) Sheldrick, G. M. *SHELXL-97: Program for the Refinement of Crystal Structures*, University of Gottingen, Germany, 1997.
(53) Mackay, S.; Edwards, C.; Henderson, A.; Gilmore, C.; Stewart, N.; Shankland, K.; Donald, A. *MaXus: a computer program for the solution and refinement of crystal structures from diffraction data*, University of Glasgow, Scotland, 1997.
(54) Waasmaier, D.; Kirfel, A. *Acta Crystallogr., Sect. A: Found. Crystallogr.* **1995**, *51*, 416.
(55) Brunold, T. C.; Tamura, N.; Kitajima, N.; Moro-oka, Y.; Solomon, E. I. *J. Am. Chem. Soc.* **1998**, *120*, 5674−5690.
(56) Kitajima, N.; Fujisawa, K.; Moro-oka, Y. *J. Am. Chem. Soc.* **1989**, *111*, 8975−8976.
(57) Park, G. Y.; Qayym, M. F.; Woertink, J.; Hodgson, K. O.; Hedman, B.; Narducci Sarjeant, A. A.; Solomon, E. I.; Karlin, K. D. *J. Am. Chem. Soc.* **2012**, *134*, 8513−8524.
(58) Do, L. H.; Hayashi, T.; Moenne-Loccoz, P.; Lippard, S. J. *J. Am. Chem. Soc.* **2010**, *132*, 1273−1275.

(59) Zhang, Y.; Furutachi, H.; Fujinami, S.; Nagamoto, S.; Maeda, Y.; Watanabe, Y.; Kitagawa, T.; Suzuki, M. *J. Am. Chem. Soc.* **2005**, *127*, 826−827.
(60) Kryatov, S. V.; Taktak, S.; Korendovych, I. V.; Rybak-Akimova, E. V.; Kaizer, J.; Torelli, S.; Shan, X.; Mandal, S.; MacMurdo, V. L.; Payeras, A. M.; Que, L., Jr. *Inorg. Chem.* **2005**, *44*, 85−99.
(61) Shannon, R. D. *Acta Crystallogr.* **1976**, *A32*, 751−767.
(62) Baldwin, M. J.; Ross, P. K.; Pate, J. E.; Tyeklar, Z.; Karlin, K.; Solomon, E. I. *J. Am. Chem. Soc.* **1991**, *113*, 8671−8679.
(63) Jacobson, R. R.; Tyeklar, Z.; Farooq, A.; Karlin, K. D.; Liu, S.; Zubieta, J. *J. Am. Chem. Soc.* **1988**, *110*, 3690−3692.
(64) Dong, Y.; Menage, S.; Brennan, B. A.; Elgren, T. E.; Jang, H. G.; Pearce, L. L.; Que, L. J. *J. Am. Chem. Soc.* **1993**, *115*, 1851−1859.
(65) Kitajima, N.; Tamura, N.; Amagai, H.; Fukui, H.; Moro0oka, Y.; Mizutani, Y.; Kitagawa, H.; Mather, R.; Heerwegh, K.; Reed, C. A.; Randall, C. R.; Que, L., Jr.; Tatsumi, K. *J. Am. Chem. Soc.* **1994**, *116*, 9071−9085.
(66) Fits to the data were obtained using the program "julX" (http://www.mpibac.mpg.de/bac/logins/bill/julX_en.php), written by Eckard Bill, Max Planck Institute for Bioinorganic Chemistry.
(67) Balch, A. L.; Chan, Y.-W.; Cheng, R.-J.; La Mar, G. N.; Latos-Grazynski, L.; Renner, M. W. *J. Am. Chem. Soc.* **1984**, *106*, 7779−7785.
(68) Fukuzumi, S.; Karlin, K. D. *Coord. Chem. Rev.* **2013**, *257*, 187−195.
(69) Van Eldik, R.; Hubbard, C. D. *Coord. Chem. Rev.* **2010**, *254*, 297−308.
(70) Bakac, A. *Adv. Inorg. Chem.* **2004**, *55*, 1−59.
(71) Lewis, E. A.; Tolman, W. B. *Chem. Rev.* **2004**, *104*, 1047−1076.
(72) Korendovych, I. V.; Kryatov, S. V.; Rybak-Akimova, E. V. *Acc. Chem. Res.* **2007**, *40*, 510−521.
(73) Karlin, K. D.; Kaderli, S.; Zuberbuhler, A. D. *Acc. Chem. Res.* **1997**, *30*, 139−147.
(74) Tine, M. R. *Coord. Chem. Rev.* **2012**, *256*, 316−327.
(75) Tshuva, E. Y.; Lippard, S. J. *Chem. Rev.* **2004**, *104*, 987−1012.
(76) Zhang, C. X.; Kaderli, S.; Costas, M.; Kim, E.; Neuhold, Y.-M.; Karlin, K. D.; Zuberbuhler, A. D. *Inorg. Chem.* **2003**, *42*, 1807−1824.
(77) Kieber-Emmons, M. T.; Riordan, C. G. *Acc. Chem. Res.* **2007**, *40*, 609−617.
(78) Hatcher, L. Q.; Vance, M. A.; Narducci Sarjeant, A. A.; Solomon, E. I.; Karlin, K. D. *Inorg. Chem.* **2006**, 3004−3013.
(79) Momenteau, M.; Reed, C. A. *Chem. Rev.* **1994**, *94*, 659−698.
(80) Rybak-Akimova, E. V. In *Physical Inorganic Chemistry*; Bakac, A., Ed.; Wiley: New York, 2012; Vol. *2*, pp 109−188.
(81) Bakac, A. *Prog. Inorg. Chem.* **1995**, *43*, 267−351.
(82) Jones, R. D.; Summerville, D. A.; Basolo, F. *Chem. Rev.* **1979**, *79*, 139−179.
(83) Wu, A. J.; Penner-Hahn, J. E.; Pecoraro, V. L. *Chem. Rev.* **2004**, *104*, 903−938.
(84) Würtele, C.; Gaoutchenova, E.; Harms, K.; Holthausen, M. C.; Sundermeyer, J.; Schindler, S. *Angew. Chem., Int. Ed.* **2006**, *45*, 3867−3869.
(85) Feig, A. L.; Becker, M.; Schindler, S.; van Eldik, R.; Lippard, S. J. *Inorg. Chem.* **1996**, *35*, 2590−2601.
(86) Kryatov, S. V.; Rybak-Akimova, E. V.; MacMurdo, V. L.; Que, L. J. *Inorg. Chem.* **2001**, *40*, 2220−2228.
(87) Lucas, H. R.; Meyer, G. J.; Karlin, K. D. *J. Am. Chem. Soc.* **2010**, *132*, 12927−12940.
(88) Fry, H. C.; Scaltrito, D. V.; Karlin, K. D.; Meyer, G. J. *J. Am. Chem. Soc.* **2003**, *125*, 4657−4663.
(89) Rybak-Akimova, E. V.; Otto, W.; Deardorf, P.; Roesner, R.; Busch, D. H. *Inorg. Chem.* **1997**, *36*, 2746−2753.
(90) Kobayashi, Y.; Ohkubo, K.; Nomura, T.; Kubo, M.; Fujieda, N.; Sugimoto, H.; Fukuzumi, S.; Goto, K.; Ogura, T.; Itoh, S. *Eur. J. Inorg. Chem.* **2012**, 4574−4578.
(91) Dong, Y.; Yan, S.; Young, V. G., Jr.; Que, L., Jr. *Angew. Chem., Int. Ed. Engl.* **1996**, *35*, 618−619.
(92) Wurtele, M. C.; Sander, O.; Lutz, V.; Waitz, T.; Tuczek, F.; Schindler, S. *J. Am. Chem. Soc.* **2009**, *131*, 7544−7545.
(93) Weitzer, M.; Schindler, S.; Brehm, G.; Hörmann, E.; Jung, B.; Kaderli, S.; Zuberbühler, A. *Inorg. Chem.* **2003**, *42*, 1800−1806.
(94) Brines, L. M.; Villar-Acevedo, G.; Kitagawa, T.; Swartz, R. D.; Lugo-Mas, P.; Kaminsky, W.; Benedict, J. B.; Kovacs, J. A. *Inorg. Chim. Acta* **2008**, *361*, 1070−1078.